Applied Catalysis B: Environmental 134–135 (2013) 222–230

Contents lists available at SciVerse ScienceDirect

Applied Catalysis B: Environmental

journal homepage: www.elsevier.com/locate/apcatb

Reductive removal of chloroacetic acids by catalytic hydrodechlorination over Pd/ZrO_2 catalysts

Juan Zhou[a], Yuxiang Han[a], Wenjuan Wang[a], Zhaoyi Xu[a], Haiqin Wan[a], Daqiang Yin[b], Shourong Zheng[a,*], Dongqiang Zhu[a]

[a] State Key Laboratory of Pollution Control and Resource Reuse, Jiangsu Key Laboratory of Vehicle Emissions Control, School of the Environment, Nanjing University, Nanjing 210093, China

[b] Key Laboratory of Yangtze River Water Environment of Ministry of Education, Tongji University, Shanghai 200092, China

ARTICLE INFO

Article history:
Received 14 October 2012
Received in revised form
21 December 2012
Accepted 4 January 2013
Available online 18 January 2013

Keywords:
Chloroacetic acids
Catalytic hydrodechlorination
Supported Pd catalyst
Metal–support interaction

ABSTRACT

Chloroacetic acids are common disinfection byproducts in drinking water and are of significant concern due to their strong carcinogenic, mutagenic and hepatotoxic effects. In the present study, the catalytic hydrodechlorination of chloroacetic acids (monochloroacetic acid, dichloroacetic acid and trichloroacetic acid) was investigated over supported Pd catalysts on SiO_2, ZrO_2, and activated carbon (AC) prepared by the impregnation method (denoted as *im*-Pd/support) and/or the deposition-precipitation method (denoted as *dp*-Pd/support). The catalysts were characterized by X-ray diffraction, transmission electron microscopy, measurement of point of zero charge, N_2 adsorption–desorption isotherm, H_2 chemisorption, and X-ray photoelectron spectroscopy. Characterization results showed that the points of zero charge of the supports varied. In contrast to *im*-Pd/ZrO_2, strong metal–support interaction was identified in *dp*-Pd/ZrO_2. Accordingly, *im*-Pd/ZrO_2 was found to be more active than *im*-Pd/AC and *im*-Pd/SiO_2, and *dp*-Pd/ZrO_2 exhibited higher catalytic activity than *im*-Pd/ZrO_2. Complete dechlorination of chloroacetic acids to acetic acid could be achieved on *dp*-Pd/ZrO_2 within 120 min of hydrodechlorination. The hydrodechlorination rate constants of trichloroacetic acid, dichloroacetic acid, and monochloroacetic acid over *dp*-Pd(1.74)/ZrO_2 were 0.22, 0.16, and 0.044 min^{-1}, respectively, reflecting an increase in dechlorination activity with increasing number of chlorine atoms in chloroacetic acids. It was further demonstrated that the catalytic hydrodechlorination was accomplished via a combined stepwise and concerted pathway for both trichloroacetic acid and dichloroacetic acid.

1. Introduction

As an effective, simple and cost-competitive disinfection method, chlorination has been widely adopted in drinking water supply [1,2]. However, chlorination inevitably leads to the formation of disinfection byproducts (DBPs) by a series of substitution, addition and oxidation reactions between the disinfection agent and dissolved organic compounds that are ubiquitous in the drinking water source [3,4]. Among the DBPs, chloroacetic acids (CAAs), including mono-, bi- and tri-chloroacetic acids, are of significant concern due to their strong carcinogenic, mutagenic and hepatotoxic effects [5,6]. Toxicity test results showed that the lowest concentrations of monochloroacetic acid (MCAA), bichloroacetic acid (DCAA) and trichloroacetic acid (TCAA) for significant toxic effects were 0.25, 2.0, and 0.4 mM, respectively, reflecting a toxic order of MCAA > TCAA > DCAA [7,8]. Additionally, CAAs were frequently detected at $\mu g\,l^{-1}$ level in drinking water [9,10]. Therefore, development of effective treatment methods to eliminate CAAs in drinking water is highly demanded for assuring safe drinking water supplies.

Reductive dechlorination has been considered as an attractive option to remove CAAs in water. For example, Hozalski et al. [11] studied the reduction of haloacetic acids by zero-valent iron and found that polyhaloacetic acids were readily reduced via a sequential hydrogenolysis mechanism; however, the dechlorination by zero-valent iron was not complete and MCAA was very recalcitrant toward the reduction. Due to the strong capability for H_2 activation, metallic Pd can be added to zero-valent iron to enhance the reduction of CAAs. Wang et al. [12] investigated the dechlorination of CAAs on Pd/Fe nanoparticles and concluded that MCAA could be effectively dechlorinated into acetic acid and the reaction activities of Pd/Fe nanoparticles were strongly dependent on the preparation method. Consistently, Li et al. [13] studied the electrocatalytic dechlorination of CAAs and found that effective dechlorination of MCAA into acetic acid could only be achieved on Pd-carbon and Pd/Fe-carbon electrodes.

* Corresponding author at: State Key Laboratory of Pollution Control and Resource Reuse, Jiangsu Key Laboratory of Vehicle Emissions Control, School of the Environment, Nanjing University, Nanjing 210093, China. Tel.: +86 25 89680373; fax: +86 25 89680596.
E-mail address: srzheng@nju.edu.cn (S. Zheng).

0926-3373/$ – see front matter © 2013 Elsevier B.V. All rights reserved.
http://dx.doi.org/10.1016/j.apcatb.2013.01.005

Liquid phase catalytic hydrogenation is a promising method to reductively remove inorganic and organic pollutants in water under ambient pressure and temperature conditions. For example, Vorlop and Tacke [14] first explored the liquid phase catalytic hydrogenation for the selective reduction of nitrate in water. Chen et al. [15,16] found that Cr(VI) and bromate in water could be readily reduced using the catalytic hydrogenation method. Schüth and Reinhard [17] verified the feasibility of the catalytic hydrodechlorination (HDC) of chlorinated aromatic compounds in hydrogen-saturated water. Additionally, some research groups systematically studied the catalytic HDC of chlorophenols on supported noble metal catalysts [18–24]. Hence, we hypothesized that effective removal of CAAs in water could be achieved by the liquid phase catalytic HDC over supported noble catalysts under ambient conditions. To the best of our knowledge, relevant study has not been reported thus far.

In the present study, supported Pd catalysts on different supports were prepared by the impregnation and/or deposition-precipitation method, and the liquid phase catalytic HDC of selected CAAs on the catalysts was investigated. The results showed that the CAAs could be readily reduced into acetic acid over the synthesized catalysts, reflecting the potential of liquid phase HDC as an effective option to remove CAAs in drinking water.

2. Experimental

2.1. Catalyst preparation

Bituminous coal-based activated carbon (Filtrasorb-300) with a Brunauer–Emmett–Teller (BET) surface area of 981 $m^2\,g^{-1}$ was purchased from Calgon Carbon Co., USA. SiO_2 (BET surface area of 132 $m^2\,g^{-1}$) were purchased from Shanghai Chem. Co. (Shanghai, China).

ZrO_2 support was prepared by the precipitation method. Briefly, under vigorous stirring 150 ml of 2.0 M aqueous ammonia solution was added slowly to 400 ml of 0.5 M aqueous $ZrOCl_2$ solution. After aging at room temperature for 2 h, the resulting precipitant was recovered by filtration, followed by washing with distilled water and drying at 105 °C for 6 h. ZrO_2 support was obtained by calcining the ZrO_2 precipitant in the air at 500 °C for 4 h.

Supported Pd catalysts with different supports (SiO_2, AC and ZrO_2) but similar Pd loading amounts were prepared by the impregnation method, and ZrO_2 supported Pd catalysts with varied Pd loading amounts were further prepared using the deposition-precipitation method. For the impregnation method, the support was impregnated by $PdCl_2$ solution under stirring for 2 h, followed by drying at 105 °C for 6 h, calcining in air at 300 °C for 4 h and reducing at 300 °C under a H_2 stream (40 ml min^{-1}) for 2 h. The resulting catalyst with ZrO_2 as the support is denoted as *im*-Pd(x)/ZrO_2, where x is the Pd loading amount (wt.%). As for the deposition-precipitation method, ZrO_2 support was suspended in $PdCl_2$ solution under stirring for 2 h. Then, 1.0 M Na_2CO_3 solution was added slowly to the suspension until pH 10.5. The resulting solid was recovered by filtration, washed thoroughly with distilled water, dried at 105 °C for 6 h, and reduced under a H_2 stream (40 ml min^{-1}) at 300 °C for 2 h. The obtained catalyst is denoted as *dp*-Pd(x)/ZrO_2, where x is the Pd content (wt.%). Prior to catalytic activity test, all catalysts were ground to pass through a 400-mesh sieve (<37 μm) to avoid possible intraparticle diffusion [25,26].

2.2. Catalyst characterization

The powder X-ray diffraction (XRD) patterns were collected in a range of 10–70° with a Rigaku D/max-RA powder diffractometer using Cu *Kα* radiation (Rigaku, Tokyo, Japan). Transmission electron microscopy (TEM) images of the samples were obtained on a JEM-2100 transmission electron microscope (JEM-2100, JEOL, Japan). N_2 adsorption–desorption isotherms were measured at −196 °C (77 K) on a Micromeritics ASAP 2020 instrument (Micromeritics Instrument Co., Norcross, GA, USA). The specific surface areas of the samples were calculated according to the BET method ($0.05 < P/P_0 < 0.25$). Prior to the measurement the samples were pretreated at 300 °C under vacuum (1.33 Pa) for 1 h. Pd contents of the catalysts were determined using an inductive coupled plasma emission spectrometer (ICP) (J-A1100, Jarrell-Ash, USA). The X-ray photoelectron spectroscopy (XPS) analysis was performed with a PHI5000 VersaProbe equipped with a monochromatized Al Ka excitation source ($h\nu$ = 1486.6 eV) (ULVAC-PHI, Japan). The C 1s peak (284.6 eV) was used for the calibration of binding energy.

The points of zero charge (PZCs) of the supports were measured using the potentiometric mass titration method [27,28]. Typically, 0.5 g of the support was suspended in 50 ml of 0.03 M KNO_3 solution at 25.0 °C, which was continuously bubbled with a N_2 flow (50 ml min^{-1}) under stirring. 0.2 ml of 1.0 M KOH solution was added to the suspension, and the mixture was equilibrated for 20 h to reach a stable pH. Then, the mixture was titrated by a 0.5 M HNO_3 solution, and the pH was monitored intermittently. The blank solution (without support) was also titrated by the same procedure.

Metallic Pd dispersion of the catalyst was measured using the H_2 chemisorption method. Briefly, 100 mg of the reduced catalyst was pressed into wafers, broken into small platelets, and loaded in a U-shaped quartz tube, in which the catalyst was activated in a H_2 flow (40 ml min^{-1}) at 300 °C for 1 h. After purging with an Ar flow (30 ml min^{-1}) for 1 h, the catalyst was cooled down to room temperature. The H_2 chemisorption was performed using the pulse titration model with H_2 partial pressure below 0.011 atm. The H_2 contents in the pulses were monitored by a thermal conductivity detector (TCD).

2.3. Liquid phase catalytic HDC of CAAs

The liquid phase catalytic HDC of CAAs was conducted under atmospheric pressure of hydrogen using a 250 ml of four-necked flask reactor with a sample port, pH-stat, H_2 inlet and condenser. The reaction temperature was stabilized at 25 ± 0.5 °C with a water-bath (SDC-6, Scientz Co., China). Typically, 30 mg of catalyst was suspended in 200 ml of 0.16 mM chloroacetic acid solution with pH pre-adjusted to 5.6. The suspension was purging with a N_2 flow (50 ml min^{-1}) under stirring (1400 rpm) for 30 min, and then the N_2 flow was switched into a H_2 flow (250 ml min^{-1}) during the reaction process. Samples were taken at selected time intervals and the catalyst particles were removed by fast filtration. The filtrate was analyzed using an Ion Chromatography (ICS1000, Dionex) with a mobile phase of 20 mM KOH solution. Catalyst activity was evaluated using the initial activity defined as the specific removal rate of chloroacetic acid within the initial 6 min. The results of two separate runs of the catalytic HDC of MCAA on *dp*-Pd(1.74)/ZrO_2 indicated a high data reproducibility (see Fig. 1S, supporting information).

3. Results and discussion

3.1. Catalyst characterization

The XRD patterns of the supported catalysts are compiled in Fig. 2S and 3S, supporting information. For the catalysts with AC and SiO_2 as the supports, diffraction peaks assigned to metallic Pd with a face centered cubic (fcc) crystallographic structure were observed at 40.2° and 46.7° [29,30]. However, diffraction peaks characteristic of metallic Pd were not identified in ZrO_2 supported Pd catalysts,

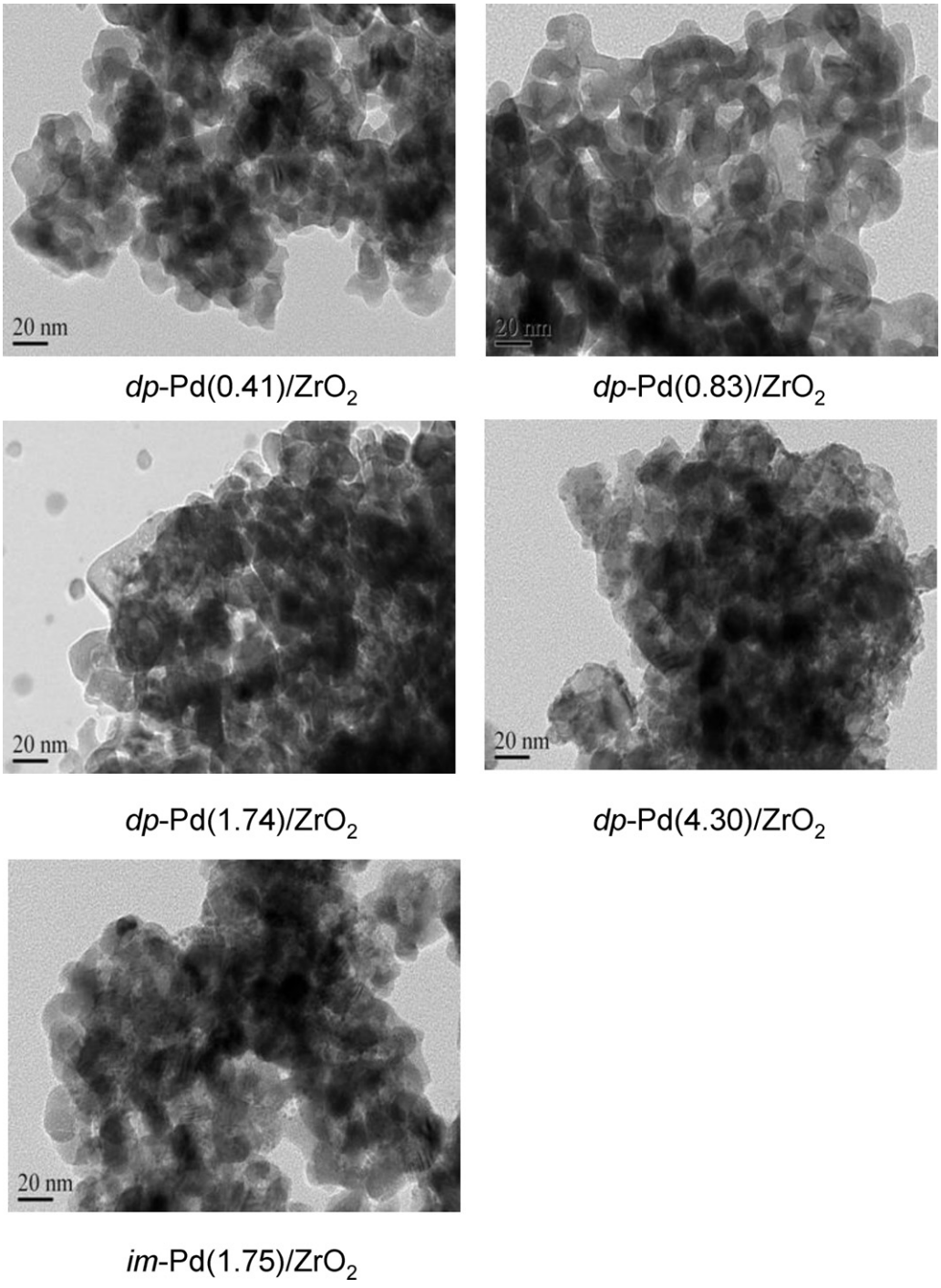

Fig. 1. TEM images of ZrO_2 supported Pd catalysts.

likely due to the high Pd dispersions (small Pd particle sizes) of the catalysts.

The PZCs of the supports were determined using the titration method and the pH curve as a function of the added HNO_3 was compared in Fig. 4S, supporting information. For all supports, the pH gradually decreased with the addition of HNO_3, while their PZCs differed markedly. The PZCs of ZrO_2, and SiO_2 were 6.3 and 3.0, respectively, but the PZC of AC was much lower than 2.0. The results were in good agreement with previous reports [28,31,32].

The TEM images of ZrO_2 supported Pd catalysts are shown in Fig. 1. In the TEM images, agglomerated ZrO_2 particles with irregular shape and sizes around 10–40 nm were decorated with ultra fine Pd particles. The average Pd particle sizes of the catalysts were further quantified based on a surface area weighted diameter [19]:

$$\overline{d_s} = \frac{\sum n_i d_i^3}{\sum n_i d_i^2} \quad (1)$$

where n_i is the number of counted Pd particles with diameter of d_i and the total number of counted particles (Σn_i) is larger than 150.

The average Pd particle sizes of the catalysts are listed in Table 1. The Pd particle sizes were found to be 1.91 nm for *dp*-Pd(1.74)/ZrO_2 and 2.26 nm for *im*-Pd(1.75)/ZrO_2, in agreement

Table 1
Properties of ZrO_2 and ZrO_2 supported Pd catalysts.

Catalyst	Pd content (wt.%)[a]	Pd dispersion (%)[b]	Pd particle sizes (nm)		BET surface area ($m^2\ g^{-1}$)
			d_1[c]	d_2[b]	
im-Pd(1.75)/ZrO_2	1.75	43.5	2.26	2.58	41
dp-Pd(0.41)/ZrO_2	0.41	72.6	1.17	1.54	40
dp-Pd(0.83)/ZrO_2	0.83	68.4	1.25	1.64	40
dp-Pd(1.74)/ZrO_2	1.74	52.8	1.91	2.13	40
dp-Pd(4.30)/ZrO_2	4.30	38.1	2.74	3.36	41

[a] Determined by ICP.
[b] Calculated from H_2 chemisorption.
[c] Calculated from TEM.

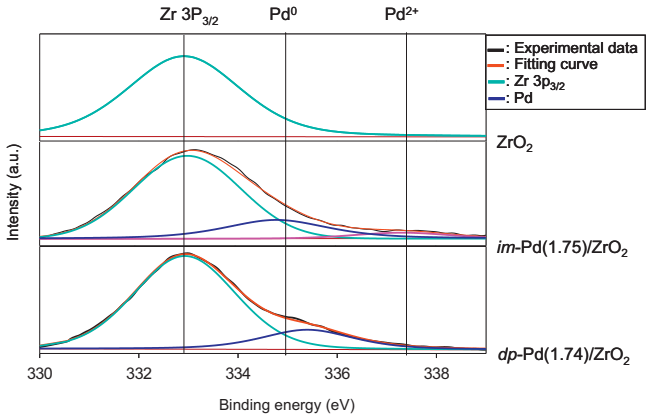

Fig. 2. XPS profiles of ZrO_2, *im*-Pd(1.75)/ZrO_2 and *dp*-Pd(1.74)/ZrO_2.

with previous conclusion that metal particle size prepared by the deposition-precipitation method is smaller than that by the impregnation method [33,34]. The average Pd particle sizes of *dp*-Pd(0.41)/ZrO_2, *dp*-Pd(0.83)/ZrO_2, *dp*-Pd(1.74)/ZrO_2, and *dp*-Pd(4.30)/ZrO_2 were calculated to be 1.17, 1.25, 1.91, and 2.74 nm, respectively, indicative of increasing Pd particle size with Pd loading.

The trend of average Pd particle sizes was also confirmed by the H_2 chemisorption results. The Pd dispersions and average Pd particle sizes of the catalysts obtained by H_2 chemisorption are listed in Table 1. The Pd dispersions of *dp*-Pd(1.74)/ZrO_2 and *im*-Pd(1.75)/ZrO_2were determined to be 52.8 and 43.5%, respectively, consistent with the results from TEM observation. Additionally, the Pd dispersions were 72.6, 68.4, 52.8, and 38.1% for *dp*-Pd(0.41)/ZrO_2, *dp*-Pd(0.83)/ZrO_2, *dp*-Pd(1.74)/ZrO_2, and *dp*-Pd(4.30)/ZrO_2, respectively, suggesting a decreased Pd dispersion with Pd loading. Alternatively, the increase of average Pd particle size with Pd loading was indicative of gradual aggregation of Pd particles on ZrO_2 surface.

The XPS spectra of *dp*-Pd(1.74)/ZrO_2 and *im*-Pd(1.75)/ZrO_2 are compared in Fig. 2. Because Pd $3d_{5/2}$ was partially overlapped with Zr $3p_{3/2}$, the XPS profiles of the samples were deconvoluted and the resulting parameters are summarized in Table 2. The binding energy of Pd $3d_{5/2}$ in *im*-Pd(1.75)/ZrO_2 was 335.0 eV, assigned to metallic Pd [35,36], while the binding energy of Pd $3d_{5/2}$ in *dp*-Pd(1.74)/ZrO_2 was observed at 335.5 eV. The higher binding energy

Table 2
Parameters of XPS spectra of ZrO_2 supported catalysts.

Catalyst	Pd $3d_{5/2}$
im-Pd(1.75)/ZrO_2	335.0
dp-Pd(0.41)/ZrO_2	335.6
dp-Pd(0.83)/ZrO_2	335.5
dp-Pd(1.74)/ZrO_2	335.4
dp-Pd(4.30)/ZrO_2	335.2

of Pd $3d_{5/2}$ in *dp*-Pd(1.74)/ZrO_2 than that in *im*-Pd(1.75)/ZrO_2 indicates the presence of cationic palladium species, attributed to the electron transfer from metallic Pd to ZrO_2 support due to the strong interaction between the two species [37,38].

The existence of strong metal–support interaction was further verified by the XPS spectra of the *dp*-Pd/ZrO_2 catalysts with varied Pd loadings (results presented in Fig. 3). For all catalysts, the binding energy values of Pd $3d_{5/2}$ were higher than that of metallic Pd (335.0 eV). Additionally, increasing Pd loading from 0.41 to 4.3 wt.% led to a shift of the binding energy from 335.6 to 335.2 eV, reflecting a gradually mitigated cationization degree of Pd with metal loading. Consistently, enhanced cationization of Pd particle with small particle size induced by metal–support interaction was previously observed on Pd/Al_2O_3 [39,40] and Pd/SiO_2 catalysts [41,42].

3.2. Liquid phase catalytic HDC of CAAs

3.2.1. Role of CAA adsorption

To test the potential mass transfer limitation, the catalytic HDC of MCAA over *dp*-Pd(1.74)/ZrO_2 with varied dosages was first conducted and the results are shown in Fig. 5S, supporting information. The HDC rate increased with catalyst dosage, while catalyst mass normalized initial activities remained nearly constant, reflecting the absence of mass transfer limitation under the reaction conditions [25,43].

For a heterogeneous catalytic reaction, reactant adsorption to catalyst surface is a prerequisite step, and the catalyst activity is likely related to the adsorption affinity for the reactant.

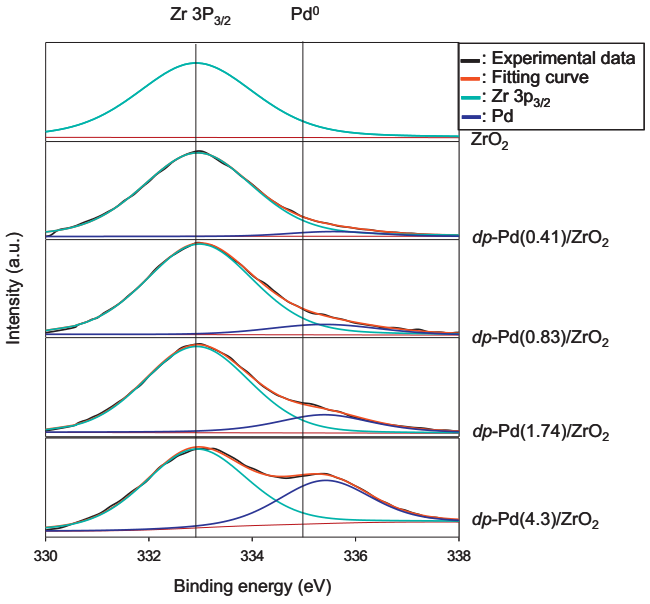

Fig. 3. XPS spectra of the *dp*-Pd/ZrO_2 catalysts.

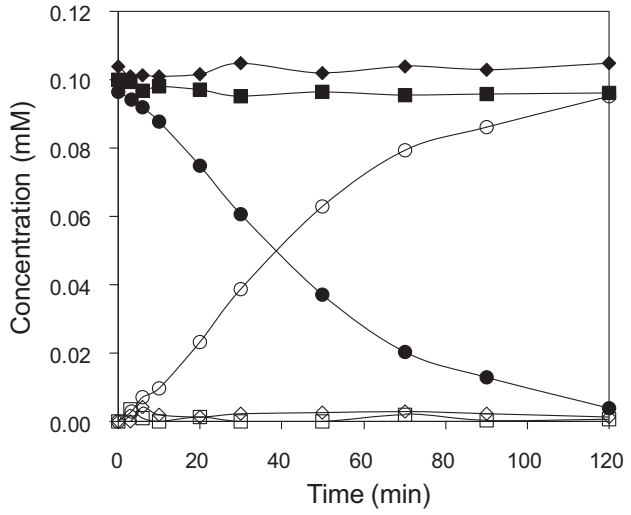

Fig. 4. Liquid phase HDC of MCAA on (● and ○) *im*-Pd(1.75)/ZrO_2, (■ and □) Pd(1.58)/SiO_2, and (♦ and ◊) Pd(1.85)/AC. Filled symbols denote MCAA concentration and open symbols denote AA concentration. Reaction conditions: pH 5.6. Catalyst dosage: 0.2 g l^{-1}, MCAA concentration: 0.1 mM.

Considering that reactant adsorption on catalyst is predominantly controlled by the support, the catalytic HDC of CAAs over supported Pd catalysts with different supports was compared. Among all examined chloroacetic acids, MCAA has the lowest reactivity toward reductive dechlorination (see more discussion below); therefore, MCAA was used as a probe molecule to test the catalytic activities of different catalysts (results presented in Fig. 4). After reaction for 120 min, negligible MCAA conversion was observed on Pd(1.58)/SiO_2 and Pd(1.85)/AC, while MCAA was removed by 95.8% for Pd(1.75)/ZrO_2. The catalytic activity is ordered as Pd(1.75)/ZrO_2 > Pd(1.85)/AC and Pd(1.58)/SiO_2. Such support-dependent catalytic activity of supported Pd catalyst was previously observed for the catalytic hydrogenation of aqueous bromate [16]. Notably, unlike the reductive dechlorination of CAAs on zero-value iron, effective dechlorination of MCAA to acetic acid could be achieved via the catalytic HDC over *im*-Pd(1.75)/ZrO_2.

As evidenced by the PZCs of the supports, at pH 5.6 *im*-Pd(1.75)/ZrO_2 are positively charged, while Pd(1.85)/AC and Pd(1.58)/SiO_2 are negatively charged. Considering that the pKa of MCAA is 2.9 [44,45], MCAA is predominated by the deprotonated anion form at pH 5.6. Hence, for Pd/ZrO_2 strong electrostatic attractive interactions exist between MCAA and the catalyst, resulting in enhanced adsorption and thus elevated HDC rate. On the contrary, for Pd/AC and Pd/SiO_2 strong repulsive interactions exist between the MCAA anion and the negatively charged catalyst surface, leading to suppressed MCAA adsorption and in turn lowered HDC activities.

The importance of MCAA adsorption was further proven by the catalytic activity dependency of *dp*-Pd(1.74)/ZrO_2 on the initial concentration of MCAA (results shown in Fig. 5). Clearly, the dechlorination efficiency increased with the initial concentration of MCAA, implying that the reaction rate was positively related to the concentration of MCAA adsorbed on the catalyst surface. The underlying mechanism could be further clarified by fitting the Langmuir–Hinshelwood model to the experimental data [46,47]:

$$r_0 = k\theta_s = k\frac{bC_0}{1+bC_0} \quad (2)$$

$$\frac{1}{r_0} = \frac{1}{kbC_0} + \frac{1}{k} \quad (3)$$

where r_0 is the initial HDC rate at MCAA concentration of C_0, θ_s is the coverage of MCAA adsorption on the catalyst surface, k is the reaction rate constant, and b is the equilibrium constant for MCAA adsorption.

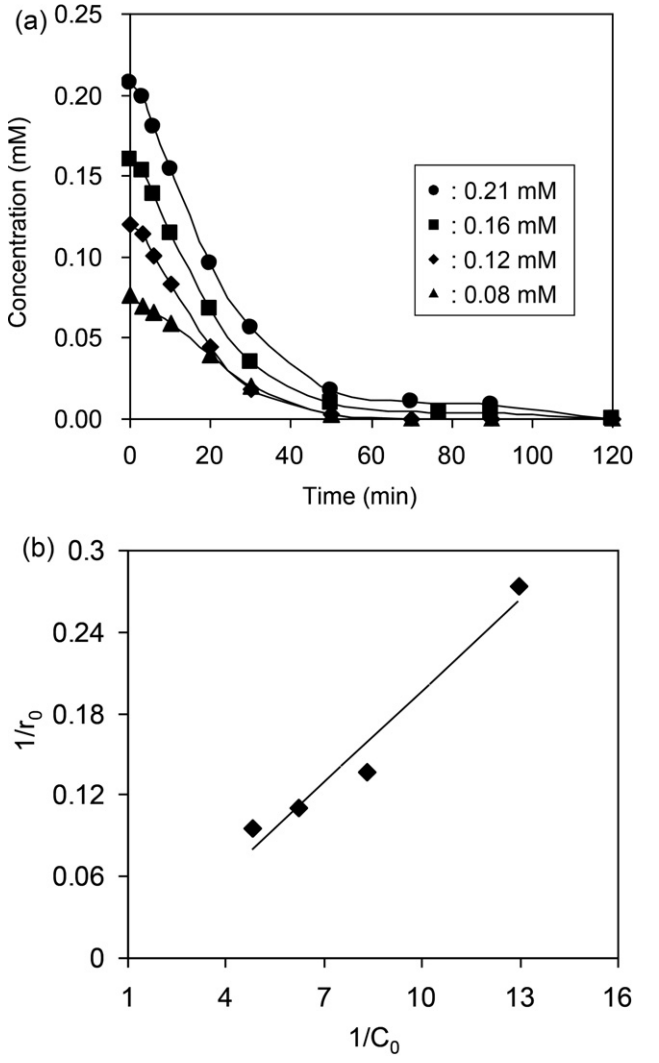

Fig. 5. (a) The catalytic HDC of MCAA at varied initial MCAA concentrations and (b) linear plot of $1/r_0$ versus $1/C_0$. Reaction conditions: pH 5.6. Catalyst: *dp*-Pd(1.74)/ZrO_2. Catalyst dosage: 0.15 g l^{-1}. Line represents the fitting curve using the Langmuir–Hinshelwood model.

Fig. 5b shows the linear plot of $1/r_0$ versus $1/C_0$ with R^2 higher than 0.96, indicating that the HDC of MCAA could be well described by the Langmuir–Hinshelwood model and the reaction was controlled by surface adsorption [47,48].

The role of MCAA adsorption was further confirmed by the influence of pH on the HDC of MCAA. The catalytic HDC of MCAA on *dp*-Pd(1.74)/ZrO_2 at varied pH is compiled in Fig. 6. After reaction for 30 min, MCAA was reduced by 7.1, 97.3 and 78.1% at pH 2.1, 4.0 and 5.6, respectively, while the conversion of MCAA was negligible at pH 8.2 (see Fig. 6a). The corresponding pH dependency of initial HDC rate is shown in Fig. 6b. Over the examined pH range of 2.1–8.2, the initial HDC rate increased with pH up to 4.0, but progressively decreased when the pH was further increased. Changing pH may prominently impact MCAA adsorption by affecting both the surface charge of catalyst and the speciation reaction of MCAA. At pH 2.1, MCAA was dominated by the molecular form (pK_a = 2.9 [44,45]), while the catalyst surface was positively charged due to the protonation effect. Accordingly, the interaction between MCAA and the catalyst was very weak, giving rise to low MCAA adsorption and thus low HDC activity. At pH 4.0, most MCAA was deprotonated

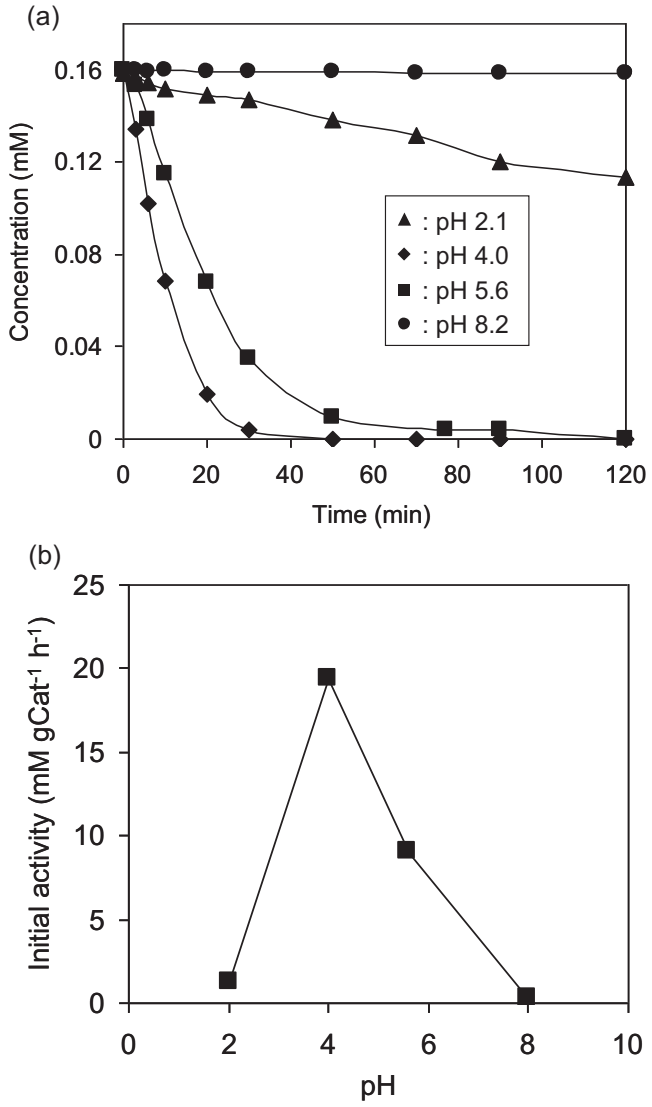

Fig. 6. (a) Influence of pH on the HDC of MCAA on *dp*-Pd(1.74)/ZrO_2 and (b) dependence of initial HDC rate on pH. Reaction conditions: Catalyst dosage: 0.15 g l^{-1}, MCAA concentration: 0.16 mM.

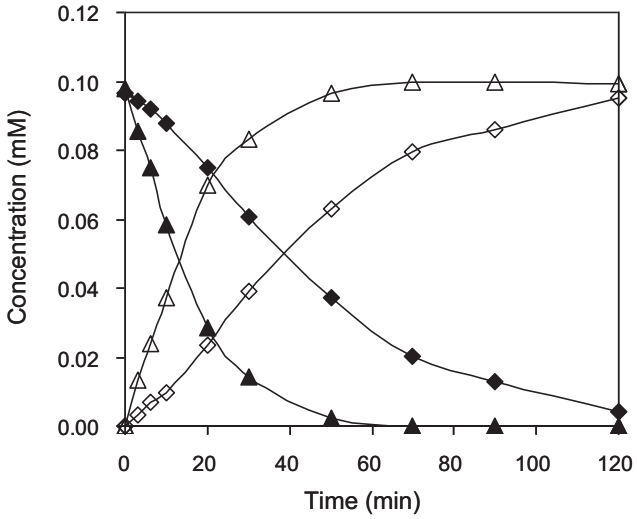

Fig. 7. The HDC of MCAA on (▲ and △) *dp*-Pd(1.74)/ZrO_2 and (◆ and ◇) *im*-Pd(1.75)/ZrO_2. Filled symbols denote MCAA concentration and open symbols denote AA concentration. Reaction conditions: pH 5.6. Catalyst dosage: 0.2 g l^{-1}, MCAA concentration: 0.1 mM.

and became negatively charged, resulting in enhanced adsorption on the positively charged catalyst surface and elevated HDC activity. However, further increase in pH made the catalyst surface negatively charged due to the deprotonation effect and generated electrostatic repulsion between the catalyst surface and the anionic MCAA molecule, leading to lowered adsorption and declined conversion of MCAA.

3.2.2. *Influence of the properties of metallic Pd*

In addition to MCAA adsorption, the HDC rate may differ with structural properties of the superficial Pd metal. To test this hypothesis, the catalytic HDC of MCAA was compared between *dp*-Pd/ZrO_2 and *im*-Pd/ZrO_2 at similar Pd loading levels (results presented in Fig. 7). After reaction for 50 min, approximately 97.4% of MCAA was removed on *dp*-Pd(1.74)/ZrO_2, while only 61.3% of MCAA was removed on *im*-Pd(1.75)/ZrO_2. The higher catalytic activity of *dp*-Pd(1.74)/ZrO_2 than that of *im*-Pd(1.75)/ZrO_2 can be well interpreted in terms of surface metal properties. In comparison with the catalyst prepared by the impregnation method, the catalyst prepared by the deposition-precipitation method has smaller metal particle size and stronger metal–support interaction [33,34]. As shown in Table 1, the average Pd particle sizes of *dp*-Pd(1.74)/ZrO_2 and *im*-Pd(1.75)/ZrO_2 were 1.91 and 2.26 nm, respectively. The strong metal–support interaction in *dp*-Pd(1.74)/ZrO_2 was verified by the positively charged Pd particles. Gomez-Sainero et al. [49] studied the catalytic HDC of CCl_4 on Pd/AC and concluded that the presence of positively charged Pd species might markedly enhance the catalytic activity by activating C-Cl bond via abstraction of nucleophilic chloride anion and formation of highly reactive $^{+}CCl_3$ ion. Consistently, Shao et al. [50] compared the catalytic performance of mesoporous carbon supported Pd catalyst (Pd/OMC) with Pd/AC for the HDC of 2,4-dichlorophenol, and attributed the higher catalytic activity of Pd/OMC to the higher content of cationic Pd. Very recently, Baeza et al. [21] concluded that the catalytic activity of nanosized Pd for the HDC of 4-chlorophenol in water was positively correlated to Pd^{n+}/Pd^0 ratio of the catalysts reduced by methanol. In this study, the presence of positively charged Pd species in *dp*-Pd(1.74)/ZrO_2 could facilitate the activation of C—Cl bond of MCAA and enhance the catalytic activity in a similar fashion.

Moreover, the supported catalyst may exhibit a prominent particle-size effect for the catalytic HDC, wherein the catalytic activity of exposed Pd site differs with Pd particle size [51,52]. In the present study, the Pd particle size in the supported catalyst was adjusted by varying Pd loading amount, and the influence of Pd loading on the catalytic HDC of MCAA is presented in Fig. 8. The HDC activity showed strong dependence on the Pd loading. At loading levels below 1.74 wt.%, the catalytic activity of *dp*-Pd/ZrO_2 increased with the Pd loading, while further increase in Pd loading did not markedly enhance the catalytic activity. More insight into the catalytic activity dependence of Pd sites on metal particle size can be gained by measuring the turnover frequency (TOF), defined as the HDC rate of MCAA per exposed Pd atom within the initial 6 min. The numbers of exposed Pd atom in the catalysts were determined by the H_2 chemisorption method. The dependence of TOF on Pd metal particle size of the catalyst is described in Fig. 8b. A volcano-type dependence of the catalytic activity of the exposed Pd atom on Pd particle size was shown. In the catalytic HDC of MCAA over supported noble metal catalyst, the activation of C—Cl bond and H_2 are proposed to be the crucial steps [49]. In general, larger Pd particles exhibit stronger catalytic ability for H_2 activation due to the enhanced H_2 solubility and the favorable formation of β-PdH phase [53,54]. On the contrary, smaller Pd particles are more susceptible to cationization owing to the enhanced metal–support interaction, as indicated by the XPS results. Therefore, increasing Pd

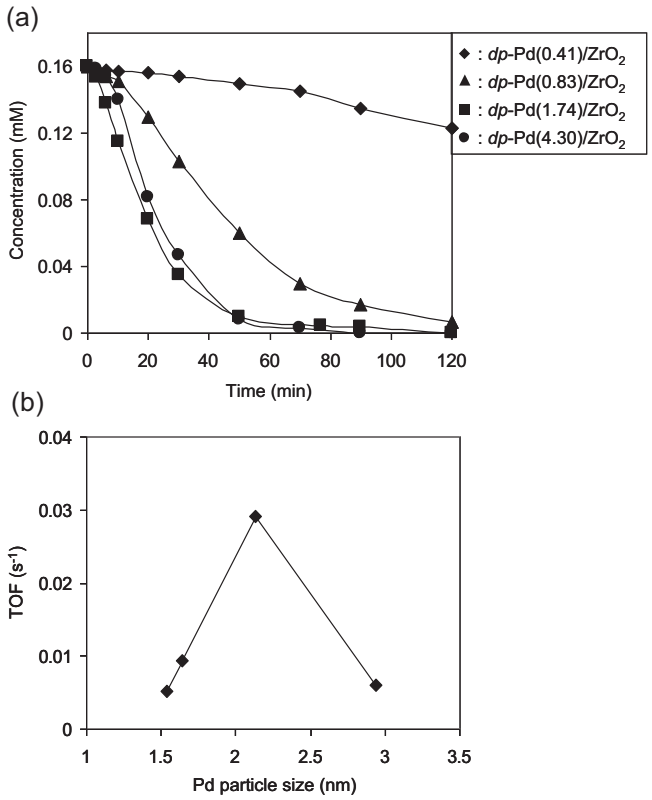

Fig. 8. (a) The HDC of MCAA on the *dp*-Pd/ZrO_2 catalysts and (b) dependence of TOF on Pd particle size. Reaction conditions: pH 5.6. Catalyst dosage: 0.15 g l^{-1}.

particle size favors H_2 activation, but inhibits C—Cl bond activation on the exposed Pd atom, and as a result a volcano-type catalytic activity-Pd particle size curve is observed.

3.2.3. Mechanism of catalytic HDC of CAAs

The catalytic HDC of MCAA, DCAA and TCAA over *dp*-Pd(1.74)/ZrO_2 is compared in Fig. 9. For DCAA and TCAA, partially dechlorinated intermediate products were identified along with the completely dechlorinated product acetic acid. For polychlorinated CAAs, the formation and decay of partially dechlorinated intermediates were likely caused by a sequential dechlorination mechanism [55,56]. It is noteworthy that MCAA was removed within about 120 min, while the dechlorination of DCAA and TCAA was accomplished within about 20 and 6 min, respectively, reflecting an increased dechlorination rate with the chlorination degree. The strong electron withdrawing ability of the chlorine atom causes the carbon center electron deficient, which is more susceptible to hydrogenation reduction [57,58]. Notably, despite different chlorination degrees MCAA, DCAA and TCAA could be completely reduced to acetic acid within approximately 120 min given similar reaction conditions, implying that MCAA reduction is the rate limitation step for complete dechlorination of TCAA and DCAA.

For polychlorinated organic pollutants, the catalytic HDC may be implemented via stepwise or/and concerted pathways [50,59], which could be verified by fitting the kinetic data [59]. For MCAA, DCAA and TCAA, the possible dechlorination pathways are depicted in Scheme 1. The respective rate constants of the HDC of CAAs were obtained by fitting the kinetic data (see details in Appendix A, supporting information), and the results are summarized in Table 3. The k_1 rate constants were 0.044, 0.16 and 0.22 min^{-1} for MCAA, DCAA and TCAA, respectively, confirming a reactivity order of TCAA > DCAA > MCAA. Notably, along with the sequential dechlorination the direct conversion of DCAA to acetic acid with

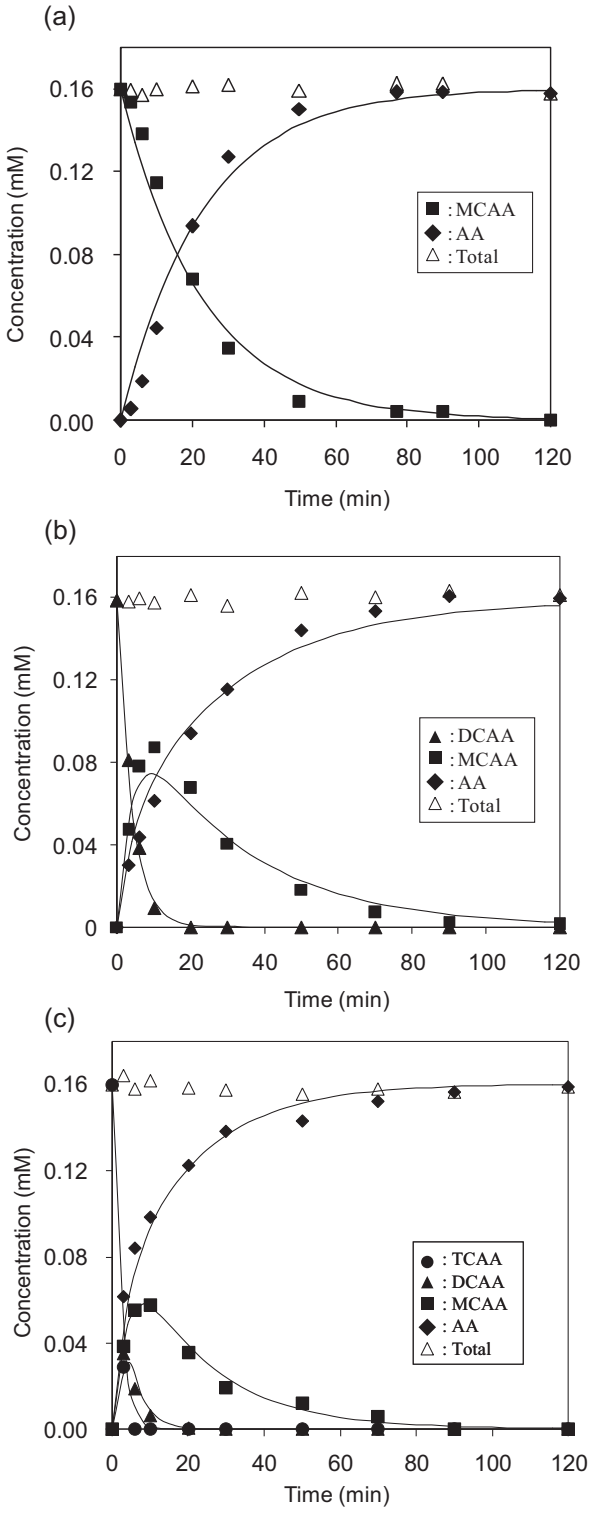

Fig. 9. The catalytic HDC of (a) MCAA, (b) DCAA and (c) TCAA on *dp*-Pd(1.74)/ZrO_2. Lines represent the fitting curves. Reaction conditions: pH 5.6. Catalyst dosage: 0.15 g l^{-1}.

a rate constant of 0.093 min^{-1} (k_2) was identified, suggesting that the HDC of DCAA is accomplished via a combined stepwise and concerted pathway. Similar results were also observed for the HDC of TCAA. Additionally, for DCAA the ratio of the rate constant of the stepwise pathway (k_1) to that of the concerted pathway (k_2) is 1.72, reflecting that the HDC is mainly controlled by the stepwise pathway. As for TCAA, the ratio of the rate constant of the stepwise

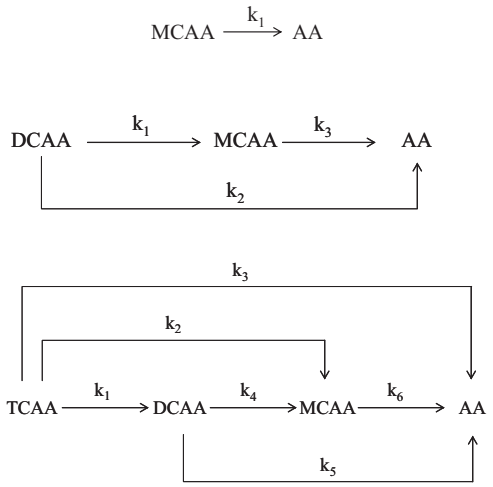

Scheme 1. Reaction pathways of the liquid phase catalytic HDC of MCAA, DCAA and TCAA.

Table 3
Fitting rate constants of the catalytic HDC of MCAA, DCAA and TCAA on *dp*-Pd(1.74)/ZrO_2.

	Catalytic HDC of MCAA	Catalytic HDC of DCAA	Catalytic HDC of TCAA
k_1 (min^{-1})	0.044	0.16	0.22
k_2 (min^{-1})	–	0.093	0.12
k_3 (min^{-1})	–	0.033	0.14
k_4 (min^{-1})	–	–	017
k_5 (min^{-1})	–	–	0.12
k_6 (min^{-1})	–	–	0.049

pathway (k_1) to those of the concerted pathways ($k_2 + k_3$) was 0.85, indicating that the concerted pathway is predominant. The results further suggest that in the catalytic HDC of CAAs the concerted pathway gradually prevails with the chlorination degree of CAA.

4. Conclusions

In the present study, a series of supported Pd catalysts were prepared and the liquid phase catalytic HDC of CAAs over the catalysts was investigated. Complete dechlorination of CAAs into acetic acid could be readily achieved on Pd/ZrO_2, and the reaction activities of CAAs increased with the chlorination degree due to the withdrawing electron nature of chlorine atom. ZrO_2 supported Pd catalyst displayed much higher catalytic activity than the catalysts with other supports (AC and SiO_2). The catalytic HDC of CAAs on Pd/ZrO_2 followed the Langmuir–Hinshelwood model, indicative of an adsorption controlled reaction mechanism. The HDC of MCAA was pH-dependent and the optimum catalytic activity was obtained at pH 4.0. Due to the existence of strong metal–support interaction, *dp*-Pd/ZrO_2 exhibited prominently higher catalytic activity than *im*-Pd/ZrO_2. A volcano-type dependence of TOF of active Pd site on Pd particle size was observed for *dp*-Pd/ZrO_2. DCAA and TCAA are proposed to be dechlorinated via a combined stepwise and concerted pathway, and the concerted pathway gradually predominates with chlorination degree. Findings in the present study clearly demonstrate the potential of using liquid phase catalytic HDC to effectively remove CAAs from drinking water.

Acknowledgements

The financial support from the Natural Science Foundation of China (no. 21277066, 21237002 and 21107043) and National High-Tech R&D Program of China (no. 2012AA062607) is gratefully acknowledged. We are indebted to the Modern Analytical Center, Nanjing University for the catalyst characterization.

Appendix A. Supplementary data

Supplementary data associated with this article can be found, in the online version, at http://dx.doi.org/10.1016/j.apcatb.2013.01.005.

References

[1] S.D. Richardson, M.J. Plewa, E.D. Wagner, R. Schoeny, D.M. DeMarini, Mutation Research 636 (2007) 178–242.
[2] R. Sadiq, M.J. Rodriguez, Science of the Total Environment 321 (2004) 21–46.
[3] P. Westerhoff, P. Chao, H. Mash, Water Research 38 (2004) 1502–1513.
[4] P.J. Vikesland, K. Ozekin, R.L. Valentine, Environmental Science & Technology 32 (1998) 1409–1416.
[5] P.C. Singer, D.A. Reckhow, Chemical oxidation, in: American Water Works Association (Ed.), Water Quality and Treatment: A Handbook of Community Water Supplies, fifth ed., McGraw-Hill, New York, 1999, pp. 223–234.
[6] Y.T. Woo, D. Lai, J.L. McLain, M.K. Manibusan, V. Dellarco, Environmental Health Perspectives 110 (2002) 75–87.
[7] M.J. Plewa, J.E. Simmons, S.D. Richardson, E.D. Wagner, Environmental and Molecular Mutagenesis 51 (2010) 871–878.
[8] E.S. Hunter, E.H. Rogers, J.E. Schmid, A. Richard, Teratology 54 (1996) 57–64.
[9] S.K. Golfinopoulos, A.D. Nikolaou, Desalination 176 (2005) 13–24.
[10] H. Zhou, X.J. Zhang, Z.S. Wang, Biomedical and Environmental Sciences 17 (2004) 299–308.
[11] R.M. Hozalski, L. Zhang, W.A. Arnold, Environmental Science & Technology 35 (2001) 2258–2263.
[12] X.Y. Wang, P. Ning, H.L. Liu, J. Ma, Applied Catalysis B: Environmental 94 (2010) 55–63.
[13] A.Z. Li, X. Zhao, Y.N. Hou, H.J. Liu, L.Y. Wu, J.H. Qu, Applied Catalysis B: Environmental 111–112 (2012) 628–635.
[14] K.D. Vorlop, T. Tacke, Chemie Ingenieur Technik 61 (1989) 836–837.
[15] H. Chen, Y. Shao, Z.Y. Xu, H.Q. Wan, Y.Q. Wan, S.R. Zheng, D.Q. Zhu, Applied Catalysis B: Environmental 105 (2011) 255–262.
[16] H. Chen, Z.Y. Xu, H.Q. Wan, J.Z. Zheng, D.Q. Yin, S.R. Zheng, Applied Catalysis B: Environmental 96 (2010) 307–313.
[17] C. Schüth, M. Reinhard, Applied Catalysis B: Environmental 18 (1998) 215–221.
[18] C. Menini, C. Park, E. Shin, G. Tavoularis, M.A. Keane, Catalysis Today 62 (2000) 355–366.
[19] G. Yuan, M.A. Keane, Applied Catalysis B: Environmental 52 (2004) 301–314.
[20] M.A. Keane, ChemCatChem 3 (2011) 800–821.
[21] J.A. Baeza, L. Calvo, M.A. Gilarranz, A.F. Mohedano, J.A. Casas, J.J. Rodriguez, Journal of Catalysis 293 (2012) 85–93.
[22] C.B. Molina, A.H. Pizarro, M.A. Gilarranz, J.A. Casas, J.J. Rodriguez, Chemical Engineering Journal 160 (2010) 578–585.
[23] E. Diaz, A.F. Mohedano, J.A. Casas, L. Calvo, M.A. Gilarranz, J.J. Rodriguez, Applied Catalysis B: Environmental 106 (2011) 469–475.
[24] C.B. Molina, L. Calvo, M.A. Gilarranz, J.A. Casas, J.J. Rodiguez, Applied Clay Science 45 (2009) 206–212.
[25] G. Yuan, M.A. Keane, Chemical Engineering Science 58 (2003) 257–267.
[26] G. Yuan, M.A. Keane, Industrial & Engineering Chemistry Research 46 (2007) 705–715.
[27] J. Vakros, C. Kordulis, A. Lycourghiotis, Chemical Communications (2002) 1980–1981.
[28] K. Bourikas, J. Vakros, C. Kordulis, A. Lycourghiotis, The Journal of Physical Chemistry B 107 (2003) 9441–9451.
[29] M.A. Ryashentseva, Russian Chemical Reviews 64 (1995) 967–983.
[30] Y.J. Xiong, J.Y. Chen, B. Wiley, Y.N. Xia, Y.D. Yin, Z.Y. Li, Nano Letters 5 (2005) 1237–1242.
[31] M. Kosmulski, Journal of Colloid and Interface Science 253 (2002) 77–87.
[32] M. Kosmulski, Journal of Colloid and Interface Science 353 (2011) 1–15.
[33] R. Gopinath, N.S. Babu, J.V. Kumar, N. Lingaiah, P.S.S. Prasad, Catalysis Letters 120 (2008) 312–319.
[34] M.A. Keane, R. Larsson, Journal of Molecular Catalysis A: Chemical 268 (2007) 87–94.
[35] D. Briggs, M.P. Seah (Eds.), Practical Surface Analysis, vol. 1: Auger and X-ray Photoelectron Spectroscopy, second ed., Wiley, New York, 1990.
[36] C.D. Wagner, A.V. Naumkin, A. Kraut-Vass, J.W. Allison, C.J. Powell, J.R. Rumble, NIST X-ray Photoelectron Spectroscopy Database, National Institute of Standard and Technology (NIST) Technology Services, United States of America, 2007.
[37] W.J. Shen, M. Okumura, Y. Matsumura, M. Haruta, Applied Catalysis A: General 213 (2001) 225–232.
[38] Y. Matsumura, M. Okumura, Y. Usami, K. Kagawa, H. Yamashita, M. Anpo, M. Haruta, Catalysis Letters 44 (1997) 189–191.
[39] N.S. Babu, N. Lingaiah, R. Gopinath, P.S.S. Reddy, P.S.S. Prasad, The Journal of Physical Chemistry C 111 (2007) 6447–6453.
[40] S. Hub, L. Hilaire, R. Touroude, Applied Catalysis 36 (1988) 307–322.

[41] M.G. Mason, Physical Review B 27 (1983) 748–762.
[42] Y.A. Ryndin, L.V. Nosova, A.I. Boronin, A.L. Chuvilin, Applied Catalysis A: General 42 (1988) 131–141.
[43] O.M. Ilinitch, F.P. Cuperus, L.V. Nosova, E.N. Gribov, Catalysis Today 56 (2000) 137–145.
[44] J.C. Hawley, N. Bampos, R.J. Abraham, J.K.M. Sanders, Chemical Communications (1998) 661–662.
[45] S.L. Dixon, P.C. Jurs, Journal of Computational Chemistry 14 (1993) 1460–1467.
[46] A. Pintar, J. Batista, J. Levec, T. Kajiuchi, Applied Catalysis B: Environmental 11 (1996) 81–98.
[47] Z.M. de Pedro, J.A. Casas, L.M. Gomez-Sainero, J.J. Rodriguez, Applied Catalysis B: Environmental 98 (2010) 79–85.
[48] X.F. Xue, K. Hanna, M. Abdelmoula, N.S. Deng, Applied Catalysis B: Environmental 89 (2009) 432–440.
[49] L.M. Gomez-Sainero, X.L. Seoane, J.L.G. Fierro, A. Arcoya, Journal of Catalysis 209 (2002) 279–288.
[50] Y. Shao, Z.Y. Xu, H.Q. Wan, Y.Q. Wan, H. Chen, S.R. Zheng, D.Q. Zhu, Catalysis Communications 12 (2011) 1405–1409.
[51] Z. Karpinski, K. Early, J.L. d'Itri, Journal of Catalysis 164 (1996) 378–386.
[52] B. Coq, F. Figuerasm, Coordination Chemistry Reviews 178–180 (1998) 1753–1783.
[53] M.A. Aramendia, V. Borau, I.M. Garcia, C. Jimenez, F. Lafont, A. Marinas, J.M. Marinas, F.J. Urbano, Journal of Catalysis 187 (1999) 392–399.
[54] M.A. Aramendia, V. Borau, I.M. Garcia, C. Jimenez, J.M. Marinas, F.J. Urbano, Applied Catalysis B: Environmental 20 (1999) 101–110.
[55] L.J. Matheson, P.G. Tratnyek, Environmental Science & Technology 28 (1994) 2045–2053.
[56] B.T. Meshesha, R.J. Chimentão, A.M. Segarra, J. Llorca, F. Medina, B. Coq, J.E. Sueiras, Applied Catalysis B: Environmental 105 (2011) 361–372.
[57] S. Arulmozhiraja, M. Morita, The Journal of Physical Chemistry A 108 (2004) 3499–3508.
[58] M.M. Scherer, B.A. Balko, D.A. Gallagher, P.G. Tratnyek, Environmental Science & Technology 32 (1998) 3026–3033.
[59] E. Diaz, J.A. Casas, A.F. Mohedano, L. Calvo, M.A. Gilarranz, J.J. Rodríguez, Industrial & Engineering Chemistry Research 47 (2008) 3840–3846.